Rheological and structural characterization of organo-hectorite dispersions: Influence of the organoclay loading

B. Merad, K. Bekkour, M. Gareche

Rheological and Structural Characterization of Organo-Hectorite Dispersions: Influence of the Organoclay Loading

B.MERAD[a,b], K.BEKKOUR[a], M.GARECHE[b]

a. ICube Research institute UMR 7357, CNRS, Université de Strasbourg, 2 rue Boussingault, Strasbourg 67000, France

b. Laboratory of Hydrocarbons Physical Engineering, Faculty of Hydrocarbons and Chemistry, University of M'Hamed Bougara -Boumerdes-, Independence Avenue 35000 Boumerdes, Algeria

Abstract:

The complex behavior of organoclay dispersions is influenced by the structure and the intermolecular interactions between clay platelets. The confinement of the clay particles is seen to be the main reason of this complex behavior because of the presence of surfactants with long alkyl chains on clay surfaces. The rheological properties of organo-hectorite (OHt) dispersed in gasoil were studied using a controlled stress rheometer. Commercial organoclay surfaces were modified with dimethyldialkyl quaternary ammonium cations. It was found that all the dispersions exhibit yield stress with a shear thinning behavior. Flow curves were correlated using both the Herschel-Bulkley phenomenological model and the Carreau-Yasuda structural model, in order to describe, respectively, the macroscopic and the microstructural behaviors of the dispersions (3 to 10 wt%). The parameters of the Carreau-Yasuda model showed the existence of a critical concentration of 6 wt%. Furthermore, frequency sweep tests showed that the dispersions start to have a fully developed gel behavior with a more pronounced solid-like structure at loadings greater than the critical concentration.

Keywords: Critical Concentration; Organoclay; Organo-Hectorite; Microstructure; Dispersion; Rheology.

1 Introduction

Modified clays or organoclays are usually made using smectite clays, in particular, sodium montmorillonite and hectorite because of their high cation exchange capacity (Murray, 2007). In the modification process (from hydrophilic to organophilic), cations present in the interlayer space like Na^+ and K^+ are replaced by organic cations such as quaternary ammoniums (Jordan, 1949). Organoclays are widely used in several applications as adsorbents of organic molecules in water/soil/air treatment, rheology control agents in paints, cosmetics, greases, oil-based drilling fluids (Murray, 2000; Chtourou *et al.*, 2006; Cavalcanti *et al.*, 2012; Ben Moshe and Rytwo, 2018; Gai *et al.*, 2019) and more recently in polymer/clay nanocomposites where organoclays, are mixed with polymers to make highly resistant materials (Paiva *et al.*, 2008; Ray, 2010; Cavalcanti *et al.*, 2012; Jayaraj *et al.*,2018; Shakeri *et al.*,2019). Some of the methods used to organically modify clay minerals are (Bergaya and Lagaly, 2002; Jaber and Miehé-Brendlé, 2009): adsorption or ion exchange of the interlayer cations with organic molecules or cations, binding of inorganic and organic anions on the edges of clay mineral layers and grafting of organic molecules.

The microscopic structure of organoclays depends on the cation density in the basal spacing, on the nature of the silicate clay mineral and on the alkyl chain length used in the modification process. Three organizations of the alkylammonium cations in the interlayer spacing are possible: (i) in monolayers (ii) in bilayers (iii) in pseudo-trimolecular layers which are observed in highly charged smectites. The type of organization of alkyl chains controls the basal spacing of the organoclay. Monolayer arrangement takes place if the equivalent area (Ae) i.e. the available clay surface for a monolayer cation configuration is larger than the area of the surfactant cation (Ac). In this case, smectites have a basal spacing of 13,6 Å. If the area

of the alkylammonium ions becomes larger than the available clay surface, a bilayer arrangement takes place with an interlayer of 17,5 Å (Lagaly, 1981). If the surfactant cation area becomes larger than twice the equivalent area, three layers structure of alkylammonium are observed. Since the latter structure is energetically unstable, the alkyl chains, in this case, form a paraffin type structure where the basal spacing depends on the angle between the clay surface and the axes of the alkyl chains (Paiva *et al.*, 2008). The method used to prepare the organoclay used in this work is ion exchange of interlayer cations with alkylammonium ions which is one of the most studied and applied clay organic modification methods (Bergaya and Lagaly, 2002; Merinska *et al.*, 2002; Ragouilliaux, 2007).

The swelling of modified clays in organic media has been largely studied by several authors (Jordan, 1949; Dekany *et al.*, 1986; Vaia *et al.*, 1994; Moraru, 2001; Burgentzlé *et al.*, 2004). The work of Jordan (Jordan, 1949) was one of the first investigations on the swelling of organoclays where it was found that the factors controlling the swelling of organoclay in organic media are the surface of the clay platelets, the degree of saturation in organic cations and the nature of the dispersing medium. Slabaugh and Hiltner (1968) and Gherardi et al. (1996) found that several parameters can influence the gelling of the organoclay in organic media such as the nature of clay, the nature of the surfactant used in the modification process, the dielectric constant of the couple clay/solvent and the presence of an alcohol or water. Lagaly and Malberg (1990) in their work showed that the presence of a polar activator in the dispersing medium has a major effect on the aggregation and the stability of organoclay dispersions. Same remarks were made by Bhat et al. (2013) where it was found that a mixture of methanol/H_2O (95/5) may be added to organo-bentonite dispersions to generate a larger hydrogen bonds network.

A number of studies have been carried out on the rheological behavior of clay dispersions in aqueous media in which clay particles show a shear thinning behavior with yield stress and a

gel behavior at low clay concentrations (Jhon *et al.*, 1996; Mourchid and Levitz, 1998; Bekkour *et al.*, 2001, 2002, 2005; Ben Azouz *et al.*,2010). Bekkour et al. (2005) investigated the time dependency of the bentonite dispersions in water where it was observed that bentonite dispersions, whose behavior was correlated with the Hershel-Bulkley model, exhibit a shear thinning thixotropic behavior. The authors showed that the thixotropy of these dispersions, which is clay concentration dependent, is due to the buildup and the breakdown of the inner structure of the dispersion. Depending on the PH of the dispersing medium, three possible clay platelets configurations are possible in clay dispersions (Benna *et al.*, 1999): face-to-face, edge-to-face, and edge-to-edge. A few authors attributed the gelling of the clay dispersions to the configuration of the clay platelets where the electrostatic attraction between the negatively charged faces and the positively charged edges leads to the formation of a 3D network termed "house-of-cards" (Benna *et al.*, 1999; Luckham and Rossi, 1999; Ramos-Tejada *et al.*, 2001; Bekkour *et al.*, 2002; Ben Azouz *et al.*,2010). Ramsay (1986) in his work on synthetic hectorite clay dispersions attributed the gelation and the viscoelastic properties of the dispersion to the swelling and the repulsion between clay platelets in the dispersing medium. One of the few studies on clays dispersed in non-aqueous media was that of Zhang et al. (2003), where the authors studied two montmorillonite clay dispersions (KSF and K10) in silicone oil. Dynamic rheological experiments showed that, depending on the type and the concentration of the clay, both dispersions exhibited a viscoelastic behavior. Shear experiments illustrated that K10 clay dispersions exhibited both a Newtonian and a shear thinning behavior depending on their clay loading.

The rheological behavior of organoclay in organic media has been less studied (Zhang *et al.*, 2003; Hato *et al.*, 2011; Bhatt *et al.*, 2013; Zhuang *et al.*, 2016, 2017, 2018; Geng *et al.*, 2019). Hato et al. (2011) investigated the rheological behavior of three commercial organo-montmorillonites (Cloisite 15A, 25A, and 30B), modified by three different quaternary

ammonium salts, dispersed in silicone oil. Cloisite 15A showed the best compatibility with the silicone oil and all the dispersions exhibited a non-Newtonian, shear thinning solid-like behavior. The study has also shown that the viscoelastic characteristics of the dispersions depend on the level of hydrophobicity of the surfactant used in the clay modification process, as the elastic characteristics were higher for the dispersions containing organoclays modified with surfactants representing higher hydrophobicity. The rheological behavior of exfoliated Cloisite 15 A dispersed in xylene was also reported by Zhong and Wang (2003) in one of the most detailed studies on the rheology of organoclay dispersions, where the yield behavior and viscoelastic properties of organoclay dispersions were studied at different concentrations. Dynamic shear measurements showed that the dispersions exhibit a gel behavior at loadings as low as 1 wt%. Furthermore, controlled stress measurements illustrated a positive correlation between the storage modulus G' and the yield stress, as a function of clay loading. Zhuang at al. (2016) studied the influence of temperature on the structure and rheology of montmorillonite modified with (cetyl trimethyl ammonium bromide) dispersed in diesel oil and heated in a rotatory oven for 16 hours at four different temperatures. Up to a critical temperature, thixotropic characteristics were found to be increasing. Beyond this critical temperature, gradual destruction of the gel structure in the dispersions was noticed, due to the desorption of the surfactants. The gelling was explained by the formation of edge-to-edge and face-to-edge configurations. The temperature was seen to affect the swelling of the organoclay where the swelling increases with the temperature until exfoliation then shrinking of the basal spacing. The same rheological behavior as a function of temperature was noticed for modified sepiolite dispersed in white oil (Zhuang *et al.*, 2018). Several phenomenological models were used to correlate organoclay dispersions rheological behavior such as the Power low model, the Casson model (Bhatt *et al.*, 2013) and the Bingham model (Zhuang *et al.*, 2016).

In the present paper, a rheological study of an organically modified hectorite (OHt) clay dispersed in gasoil is reported. To the author's knowledge, very few studies could be found on the rheological behavior of OHt dispersed in organic media (Geng *et al.*, 2019). The aim of this study is to deeply investigate the rheological behavior of OHt dispersions at loadings from 3 wt%, under which OHt dispersions in gasoil exhibit a Newtonian behavior, up to 10 wt%.

2 Materials and methods

2.1 Materials

The clay used for the experiments is Bentone 38, an organically modified hectorite clay manufactured by Elementis Specialties UK. Hectorite is a member of the smectite clay family and can swell and exfoliate in water. The used hectorite is from hydrothermal origin with a unit cell formula: $Na_{0,74}[Mg_{5,33}\ Li_{0,60}](Si_{7,98}\ Al_{0,02})O_{20}\ \ F_{2,69}(OH)_{1.31}$. It belongs to the phyllosilicate 2:1 family which is formed by an octahedral layer sandwiched between two tetrahedral layers (Bergaya, Theng and Lagaly, 2006; Murray, 2007). The hectorite platelets are more or less uniform and elongated in shape as they crystalize along a preferred axis. OHt platelets of the Bentone 38 are characterized with a thickness ranging from 0,002 to 0,004 µm and a length ranging from 0,005 to 1 µm (Ragouilliaux., 2007). Bentone 38 is modified by replacing the interlayer cations of hectorite by a quaternary ammonium salt cation (dimethyldialkyl quaternary ammonium cation). The modification of clay surfaces has got a lot of attention recently considering its major role in manufacturing organoclays used in numerous applications. The dispersing medium used in this work is a gasoil purchased from Total, France.

2.2 Preparation of the organoclay dispersions

147 Clay dispersions with mass concentrations of 3 to 10 wt% were studied. The dispersion
148 medium is a gasoil. Given that the preparation protocol has a big influence on the
149 reproducibility of results, an identical procedure was used to prepare all the dispersions.
150 Organoclay powder was first dispersed in gasoil and homogenized under a constant mechanic
151 agitation at 500 rpm, which was found to be the optimum speed for the preparation of
152 organoclay dispersions (Bhatt *et al.*, 2013), for 24 h. The prepared dispersions were then left
153 at rest for 24 h at 20° C and stirred at low speed for 1 h before each experiment to ensure their
154 homogenization.

155 Particle size distribution of a 3 wt% OHt dispersion was measured using the light scattering
156 technique with a Malvern Instrument Mastersizer 3000 system. The dispersion was submitted
157 to ultrasound excitations in order to avoid the formation of microgels. It was made sure to
158 apply the ultrasound excitations for short periods in order to avoid the overheating of the
159 organic medium. The particle size of the dispersion was ranging from 2 to100 μm with a
160 symmetric distribution on a semi-logarithmic scale at about 15 μm.

161 **2.3 Experimental procedures**

162 A controlled stress rheometer (AR2000, TA Instruments), equipped with a cone-and-plate
163 geometry (diameter: 60 mm; angle: 2°), was used to perform all the measurements. The
164 temperature was controlled using a Peltier system, and all measurements were conducted at a
165 constant temperature of 20.0±0.1 °C. Given that the concentration has a considerable
166 influence on the rheological characteristics of the dispersion, all the measurements were
167 conducted in an oil-saturated environment in order to prevent evaporation of the dispersing
168 phase. Aging measurements were performed in order to investigate the temporal stability of
169 the rheological parameters of OHt dispersions. The required time to reach the equilibrium
170 state, where all the rheological parameters of the dispersion remain stable during time, was
171 found to be 10 hours. The plate of the geometry was covered by a rough surface (sandpaper)

with a roughness of 30,2 μm to prevent wall slipping. Three experimental procedures were conducted to obtain the results presented in this work: (1) shear flow experiments from which flow curves were obtained by applying a continuous increasing shear stress ramp with a slop of 0,034 $Pa.s^{-1}$, (2) oscillatory measurements from 10^{-3} to 10^{2} Hz, with an applied stress belonging to the linear domain, obtained through stress sweep measurements at fixed frequencies and confirmed by the superposition of the compliance values for each concentration, (3) creep measurements for 180 s at stresses belonging to the linear domain followed by recovery for 180 s. Since OHt dispersions are very sensitive to the deformation history, the same procedures were followed for all the dispersions. In order to avoid memory effects, a preshear was applied to all samples followed by a rest under the measurement geometry, prior to the experiments.

3 Results and discussion

3.1 Shear measurements

Shear measurements of OHt dispersions in gasoil, at different concentrations, were plotted in a linear scale (Fig. 1). It could be clearly observed that OHt dispersions in gasoil exhibited a shear thinning behavior, with yield stress that increased with the OHt concentration. The rise of yield stress could be explained by the increase of the interactions between the organo-clay platelets which led to the formation of a 3D structure. This structure was the cause of the solid-like behavior of the dispersion at low shear rates. The experimental data were correlated using the Herschel-Bulkley phenomenological model, which was widely used to model the rheological behavior of the drilling fluids(Kelessidis *et al.*, 2006; Baba Hamed and Belhadri, 2009; Rooki *et al.*, 2012):

$$\sigma = \sigma_y + K\dot{\gamma}^{\alpha} \qquad (1)$$

Where σ is the shear stress at a particular shear rate $\dot{\gamma}$, σ_y is the yield stress, K is the consistency index and α is the flow index. The fits to the experimental data using the Hershel-Bulkley model were reported as solid lines in Fig. 1. The corresponding parameters of the model were listed in Table 1. The values of the yield stress were found to be increasing with the OHt loading, whereas the consistency index, K, increased up to a 5 wt% concentration and then remained constant at around 0,4 $Pa.s^{-1}$. The flow index, α, remained more or less constant, and it tended towards unity at highly concentrated OHt dispersions.

It could be noticed that the Hershel-Bulkley model best fitted the experimental data of the dispersions where the loading was lower than 6 wt%. Above this concentration, the linear plot of the shear flow measurements tended more towards a linear configuration (Bingham model). Yield stress values of the Hershel-Bulkley model will be further used in the next section.

Even though the Hershel-Bulkley model was widely used for its simplicity and satisfying results, it did not give enough information on the structural state of the studied dispersions. Furthermore, it could be noticed that it did not fit well at low shear rates and high concentrations. In order to take a deeper look into the inner structure of the OHt dispersions, the experimental data were plotted over a log-log scale. Figure 2 plots the same data as in Fig.1 in terms of the apparent viscosity as a function of shear rate. Four different regions could be noticed: (i) wall slipping phenomena at low shear rates, only noticeable at the lowest OHt loadings (3, 4 and 5 wt%), with an inflection point separating it from the second region. This behavior was related to the wall slipping of the less concentrated dispersions because of the absence of roughness on the cone surface. As the OHt dispersions became more concentrated i.e. above 5 wt%, a higher friction was applied on the smooth cone surface which led to the elimination of the wall slipping phenomena. Figure 6 of the following section reflects better the wall slipping effect in the beginning of the flow for the 3, 4 and 5 wt% dispersions. (ii) first Newtonian plateau at low shear rates. In their work on oil-based drilling

fluids, Herzhaft et al (Herzhaft *et al.*, 2003) showed that this quasi-Newtonian behavior is due to the high level of elasticity of the fluid at low shear rates. At rest, the fluid developed a solid-like structure which made it move as a single bloc at low shear rates; (iii) power law region with a power low index inferior to 1. The latter showed that the dispersion started to flow beyond the transition zone and that the elasticity of the material was diminishing. It is admitted that the shear thinning behavior of clay dispersions was due to the breakdown of the connections between the clay platelets, which led to the destruction of the inner 3D structure. This shear thinning behavior continued until the total destruction of the inner structure of the OHt dispersions and the orientation of clay platelets in the direction of the flow; (iv) second Newtonian plateau at high shear rates corresponding to the totally broken inner structure of the dispersion. It should be noted that a second Newtonian plateau was not fully developed for all the concentrations. The transition from the power law shear thinning behavior to the second Newtonian plateau occurred at higher shear rates as the concentration of the OHt dispersions increased.

Above a shear rate corresponding to the beginning of the first Newtonian plateau, all OHt dispersions expressed the same tendency i.e., two Newtonian plateaus separated by a power low behavior. Starting from this shear rate, the flow behavior was correlated using the Carreau-Yasuda structural model (Fig. 2):

$$\frac{\eta(\dot{\gamma}) - \eta_{\square}}{\eta_0 - \eta_{\square}} = [1 + (\square\dot{\gamma})^a]^{\frac{n-1}{a}} \qquad (2)$$

Where $\eta(\dot{\gamma})$ is the viscosity at any given shear rate $\dot{\gamma}$, η_0 and $\eta_{\square}$ are the zero and the infinite shear rate viscosities, $\square$ is a time constant describing the transition between the first Newtonian plateau and the shear thinning behavior, n is the power low exponent which indicates the dependency of the viscosity on the shear rate, and a is a dimensionless transition factor, describing the width of the transition zone between the first Newtonian plateau and the

power law behavior (a low value of a lengthens the transition while a high value leads to a sharp transition).

Since the Carreau-Yasuda model was not developed for yield stress fluids, it was made sure to use it after the fluid start getting sheared (i.e. after yielding). It should be also noticed that the second Newtonian plateau was not fully developed for all the concentrations, and thus the viscosity at a shear rate of 1000 s^{-1} was considered to fit all the curves. Furthermore, all the fits started from the first Newtonian plateau and the first shear thinning region, noticed at low OHt loadings, was not considered in the fitting process. The reciprocal of the time constant, $1/$ □ , corresponded to the critical shear rate from which a shear thinning behavior was observed.

The fits to the experimental data using the Carreau-Yasuda model were reported as solid lines in Fig. 2. The resulting parameters were reported in Table 2. Zero and infinite shear rate viscosities η_0 and $\eta_{\square}$ were found to be increasing with the OHt concentration. This could be explained by the increase in the interactions between organoclay platelets as the concentration increased. The time constant □ was found to be decreasing with the increase in the concentration of OHt, which indicated that the viscosity became a stronger function of the shear rate as the concentration decreased. A possible explanation of this phenomenon was the fact that the formation of an inner structure between clay platelets, and thus the energy needed to break this structure, increased as the OHt concentration increased. Similarly, as the OHt concentration got lower, less energy was needed to break the solid-like structure; a small change in the shear rate could cause high deformation of the structure. The power law exponent n, on the other hand, was found to be decreasing with the increase in the concentration of OHt. This decrease was due to the rise of the shear thinning behavior of the OHt dispersions as the concentration increased. The values of the reciprocal of the Carreau-Yasuda model time constant □ were plotted in Fig.2. This parameter could be considered as a critical shear rate, $\dot{\gamma}_c = 1/\square$, which separated the Newtonian and the shear thinning

behaviors. The critical shear rate shifted towards higher shear rates as the OHt concentration was increased, and the $\dot{\gamma}_c$ curve exhibited a slope change at a concentration of 6 wt%. To the author's knowledge, this behavior was not reported before in the literature. A similar change of slope was recorded on polymer solutions correlated using the Cross model (Benchabane and Bekkour, 2008; Ebagninin *et al.*, 2009), where the corresponding concentration was a critical concentration delimiting the semi-diluted entangled network and the concentrated network solution. In order to ensure its existence and understand the significance of this slope change in the organoclay dispersions, the parameters of the Carreau-Yasuda model were plotted as a function of the OHt concentration. In Fig. 3, the reciprocal of the time parameter of the Carreau-Yasuda model was plotted as a function of the OHt loading. In the same figure, and for clarity purposes, the reciprocal of the zero-shear-rate viscosity was plotted. Both the curves of $1/\square$ and $1/\eta_0$, as a function of the OHt concentration, exhibited a slope change at the same concentration reported above, i.e. 6 wt%. Up to this concentration, the rate of change of both the zero-shear-rate viscosity and the time constant seemed to be higher than for concentrations above 6 wt%. The latter concentration could be considered as a critical one, for the couple OHt-Gasoil dispersions. This concentration c* corresponded to the concentration at which the OHt platelets swell and absorb all the available dispersing media. As of this concentration, all the dispersing media was absorbed by the OHt platelets and the dispersion became overcrowded which allowed the swelled OHt platelets to form a more complex 3D solid-like structure.

Using the Carreau-Yasuda model parameters mentioned in Table. 2, the dimensionless viscosity, $(\eta - \eta_{\square})/(\eta_0 - \eta_{\square})$, was plotted as a function of the dimensionless shear rate, $\square\dot{\gamma}$. It was noticed that, starting from a 6 wt% OHt loading, all the curves of the dimensionless viscosity as a function of the dimensionless shear rate superposed (Fig.4). The latter indicates that all the OHt dispersions with concentrations higher than the critical concentration c* had a

similar microstructural behavior, which was different from the behavior corresponding to loadings lower than c*. Furthermore, it was possible to fit all the experimental data with a Carreau-Yasuda model master curve (Fig.4).

3.2 Yield Behavior:

The purpose of this section was to determine the yield stress of OHt in gasoil dispersions at different concentrations and to follow its evolution as a function of OHt loading. In order to determine the yield stress, a continuous shear stress ramp was applied until the flow of each sample. Strain and shear rate were recorded as a function of time. Figure 5 illustrated the experimental data for a 6 wt% (a) and an 8 wt% (b) OHt dispersions.

The yield stress was determined as the stress corresponding to the drastic change of the curves representing the strain and the shear rate as a function of time. When this change occurred, the sample was considered to start flowing and the yield stress was reached. When comparing the curves before yield stress, it could be noticed that, though the sample deformed, the shear rate stayed more or less constant. In this domain of stresses, the sample did not flow and behaved like a solid due to its elastic properties. After reaching the yield stress, the sample flowed and the deterioration of its inner structure begun. Repeating the same protocol at all clay loadings, yield stresses σ_y as a function of OHt loading were obtained. To ensure the validity of these values, apparent viscosity $\eta = \sigma/\dot{\gamma}$ was plotted as a function of the applied stress for all the OHt concentrations in Fig. 6.

The different curves illustrated the same regions as in the previous section. In this work, the shear stress, corresponding to the transition from the first Newtonian plateau to the shear thinning region, was considered to be the yield stress. In the range of the measured viscosity, it could be noticed that the apparent viscosity exhibited a Newtonian plateau with the increasing shear stress up to the point of yield in Fig. 6, where the viscosity dropped as much

318 as 2 orders of magnitude as the shear stress kept increasing until reaching the second
319 Newtonian plateau. The transition occurred at higher shear stresses as the OHt concentration
320 increased.

321 Yield stresses from experimental data and the Hershel-Bulkley model were plotted on the
322 same graph in Fig. 7. Unexpectedly, a small difference could be noticed between yield stress
323 values from the Hershel-Bulkley model and those from the experimental data. Flow
324 measurement yield point values were slightly higher than those of Herschel-Bulkley except
325 for the two lowest concentrations (3 and 4 wt%). This validated the use of the simple Hershel-
326 Bulkley model as a method to rapidly obtain the values of the yield point. It is noteworthy that
327 the curve of the measured yield point stresses on Fig.7 exhibited a change of slope at a
328 concentration of 6 wt% of OHt in gasoil dispersions. This change of slope confirmed the
329 observations made in the previous section. Zhong and Wang (2003) in their work, attributed
330 the cause of the viscosity difference, between the rest and the fully broken states of
331 organoclay dispersions at high clay loadings, to the formation of a network between clay
332 platelets due to their confinement in the dispersing media, which leads to a gel behaving as an
333 elastic solid. The formation of Hydrogen bonds between organoclay platelets, on the other
334 hand, was seen to be unlikely to happen because of the high distances between clay platelets
335 due to the presence of the long quaternary ammonium chains on the clay surfaces.

336 **3.4. Viscoelastic properties:**

337 In the previous sections, the existence of a critical concentration, c*, was put in evidence. It
338 was hypothetically related to the formation of an inner network of OHt platelets due to the
339 absorbance of all the dispersing media and the decreasing spaces between clay platelets as the
340 concentration increased. In order to investigate the latter hypothesis, dynamic and creep
341 experiments were performed, as they allow for the investigation of the viscoelastic properties
342 of the OHt dispersion under conditions near to at-rest state. These tests deform the gel

structure of the OHt dispersions without breaking their inner structure. Furthermore, it was made sure that all the tests were carried out in the linear domain of the OHt dispersions.

The experiments consisted first, of the oscillatory tests. As the interest is on the elastic properties of the OHt dispersions, and for clarity purposes, only the storage modulus, *G'*, as a function of the frequency was reported in Fig. 8. The measurements were performed by applying a constant stress, belonging to the linear domain of each concentration, and a continuous descending frequency sweep along five decades (10^2 to 10^{-3} Hz). It was quite interesting to observe the tendency of the curves of the storage modulus, G', of OHt dispersions. Two remarks could be made from Fig. 8: (1) depending on its concentration, the curves of G' of the OHt dispersions showed two different behaviors. The first for the lowest OHt concentrations (3 and 4 wt%) where the domain of linearity was very narrow, along which the storage modulus values increased without reaching a plateau. It could be concluded that, at low concentrations, OHt dispersions did not behave as a gel. The second behavior was the gel behavior, where a constant plateau of G' appeared on large frequency ranges for the rest of the OHt concentrations. This behavior indicated that the dispersions behaved as an elastic solid under low stresses. This solid-like structure could only be due to the inner architecture of the OHt platelets, in a way that the energy needed to separate clay particles became higher than the energy resulting from the oscillatory shear. (2) Although having a gel behavior, 5 wt% OHt dispersions exhibited a narrower linearity domain than the higher concentrations; it could be also noticed that its corresponding storage modulus was near, in value, to those of the 3 and the 4 wt%.

In addition to the oscillatory properties discussed above, creep tests were carried out. Each sample was first crept, for 180 seconds within its linear domain, then it was allowed to recover for an additional 180 seconds. The strain was measured for each experiment and compliance $J(t)$ values were deducted:

$$J(t) = \frac{\gamma(t)}{\sigma} \quad (3)$$

Where $\gamma(t)$ is the measured strain and σ is the applied stress.

To ensure the linear behavior of the dispersions, at least three tests were performed on each concentration using different stress values belonging to the linear domain, and it was made sure that the compliance values of all the tests overlapped for each concentration. The elastic properties of the dispersions were defined by fitting the experimental results using the Burger model, for the creep data, which associated in series a Maxwell and a Kelvin Voigt models(Dolz *et al.*,2008):

$$J(t) = \frac{1}{G_1} + \frac{1}{G_2}\left[1 - exp\left(\frac{-tG_2}{\eta_2}\right)\right] + \frac{t}{\eta_1} \quad (4)$$

Where G_1 and G_2 are the elastic moduli of the Maxwell and the Kelvin-Voigt units of the model, respectively. η_1 the residual viscosity related to dashpot of the Maxwell unit and η_2 the internal viscosity associated with the Kelvin-Voigt model.

The recovery experimental data, on the other hand, were correlated using the Weibull distribution function (Jia *et al.*, 2011):

$$J(t) = J_{\square} + J_{KV}\, exp(-Bt^C) \quad (5)$$

Where $J_{\square}$ is the full recovery of the material, J_{KV} is the proper recovery of the material occurring after the instantaneous elastic recovery, and the parameters *B* and *C* describe the recovery speed of the material.

Compliance values at $t = \square$ and $t = 180s$ were calculated using Equations (4) and (5), then the elastic index ΔJ was deduced:

$$\Delta J = J(180) - J_{\square} \quad (6)$$

389 Storage modulus values, G', from the oscillatory measurements, took at a frequency of 0,1 Hz,
390 and the elastic index, ΔJ, were plotted as a function of the OHt concentration in Fig. 9. The
391 storage modulus, *G'*, reflected the elastic properties of the OHt dispersions, and it was directly
392 related to its inner structure. The increase of *G'* was proportional to the increase of the
393 attractive forces keeping the OHt platelets connected to each other and behaving like a solid.
394 According to Fig. 9, which illustrated the evolution of *G'* and thus the inner structure as a
395 function of the clay loading, the curve of *G'* underwent a slope change at the same critical
396 concentration, c*, observed in the previous sections. Because *G'* was related to the inner
397 structure of the OHt dispersion, it could be concluded that a drastic change related to the
398 network of OHt particles occurred at c*. In addition, it could be noticed that the curves of ΔJ
399 exhibited a knee-point at the same critical concentration noticed earlier i.e. $c* = 6$ wt%.

400 It is worth mentioning that these results matched with those of modified montmorillonite
401 dispersed in xylene (Zhong and Wang, 2003), except that OHt dispersions expressed lower
402 magnitudes of viscosity and elastic modulus. Zhong and Wang (2003) described the storage
403 modulus values *G'* of the modified montmorillonite dispersions as "sharply increasing" at low
404 concentrations and then "leveling-off" at higher ones.

405 To further investigate this theory, OHt in gasoil dispersions were prepared at the same
406 concentrations and conditions studied above. The same volume, of 50 ml of each
407 concentration, was added into a graduated cylinder and kept in rest for 48 hours. The volume
408 of the gel was then measured for each concentration. The volume of the gel as a function of
409 the OHt concentration was reported in Fig. 10. The curve of the gel volume exhibited a slope
410 change at 6 wt%. After this concentration, i.e. $c* = 6$ wt%, the gel volume became more or
411 less constant and approached the total volume of the dispersion. These results supported the
412 assumption made above and the slope change could be clearly related to the change in the

413 inner structure of the OHt dispersions and thus corresponded to a critical concentration as
414 explained above.

415 4 Conclusions

416 The rheological behavior of a commercial hectorite, modified with dimethyldialkyl
417 ammonium cations, dispersed in gasoil was investigated. In order to study the viscous and the
418 elastic properties of the organo-hectorite dispersions, at concentrations going from 3 to 10
419 wt%, a stress-controlled rheometer was used to conduct shear, dynamic and creep
420 measurements. Shear flow measurements highlighted the shear thinning behavior of the
421 organo-hectorite dispersions. All studied concentrations exhibited a yield stress and its value
422 increased with the concentration in the organo-hectorite. The values of the yield stress for the
423 lowest OHt concentrations were low (ranging from 0,1 Pa at 3 wt% to 0,9 Pa at 5 wt%),
424 compared to the dispersions at higher concentrations (ranging from 2,15 Pa at 6 wt% to 22,4
425 Pa at 10 wt%). The linear plot of the shear stress as a function of the shear rate was found to
426 be well fitted, especially at low concentrations and high shear rates, with the simple Hershel-
427 Bulkley phenomenological model. The log-log plot of the viscosity as a function of the shear
428 rate illustrated that the rheological behavior of the OHt dispersions could be divided into three
429 regions (two Newtonian plateaus at low and high shear rates separated by a shear thinning
430 region). The experimental results were found to be well described by the five parameters
431 model of Carreau-Yasuda. The curve of the reciprocal of the time constant of the Carreau-
432 Yasuda model, plotted on the viscosity curve, highlighted the possibility of the existence of a
433 critical concentration at which a change in the inner properties of the dispersions occurs. The
434 plots of the Carreau-Yasuda parameters, i.e., the reciprocals of the time constant and the zero-
435 shear-rate viscosity as a function of clay loading, allowed to identify the same critical
436 concentration, c*, noticed on the viscosity curve. The curves of the yield stress, the storage
437 modulus and the elastic index, as a function of clay loading, confirmed the existence of a

438 critical concentration, c*, at which the spaces between clay platelets become very narrow and
439 a more complex 3D solid like structure occurs at rest. Using the measurements of the gel
440 volume as a function of clay loading, this critical concentration, c*, was related to the
441 confinement of the dispersing medium, based on the explanation of Zhong and Wang (2003),
442 where it was seen that it was unlikely for the organoclay platelets to form hydrogen bonds
443 because of the large spaces between the platelets due to the presence of the long alkyl chains
444 on their surfaces.

445 Based on the results presented in this work, the following explanation can be considered: at
446 low loadings, organo-hectorite platelets absorb the organic solvent and swell to their
447 maximum potential with low interactions between clay aggregates. After reaching a critical
448 concentration, the spaces between the swelled organoclay units become narrower, because of
449 the lack of the free solvent, and thus the interactions between the swelled organoclay particles
450 increase and a more complex structure takes place.

451 **References**

452 Ben Azouz K., Dupuis, D., Bekkour, K., 2010. Rheological characterizations of
453 dispersions of clay particles in viscoelastic polymer solutions. Appl. Rheol. 20,
454 13041.

455 Baba Hamed, S., Belhadri, M., 2009. Rheological properties of biopolymers drilling
456 fluids. J. Pet. Sci. Eng. 67, 84– 90.

457 Bekkour, K., Ern, H., Scrivener, O., 2001. Rheological characterization of bentonite
458 suspensions and oil-in-water emulsions loaded with benton Rheological Characterization of
459 Bentonite Suspensions and Oil-In-Water Emulsion Loaded With Bentonite. Appl. Rheol. 11,
460 178-187.

461 Bekkour, K., Kherfellah, N., 2002. Linear Viscoelastic Behavior of Bentonite-Water
462 Suspensions. Appl. Rheol.12, 234–240.

463 Bekkour, K., Leyama, M., Benchabane, A., Scrivener, O., 2005. Time-dependent
464 rheological behavior of bentonite suspensions: An experimental study. J. Rheol. 49,
465 1329–1345.

466 Benchabane, A., Bekkour, K., 2008. Rheological properties of carboxymethyl cellulose
467 (CMC) solutions. Colloid Polym. Sci. 286, 1173–1180.

468 Benna, M., Kbir-Ariguib, N., Magnin, A., Bergaya, F., 1999. Effect of pH on
469 Rheological Properties of Purified Sodium Bentonite Suspensions. J. Colloid Interface
470 Sci. 218, 442–455.

471 Bergaya, F., Lagaly, G., 2001. Surface modifications of clay minerals. Appl. Clay Sci. 19, 1–
472 3.

473 Bergaya, F., Theng, B.K.G., Lagaly, G., 2006. Handbook of Clay Science, First Edition.
474 Elsevier.

475 Bhatt, J., Somani, R.S., Mody, H.M., Bajaj, H.C., 2013. Rheological study of
476 organoclays pre- pared from Indian bentonite: effect of dispersing methods. Appl. Clay
477 Sci. 83-84, 106–114.

478 Burgentzlé, D., Duchet, J., Gérard, J.F., Jupin, A., Fillon, B., 2004. Solvent-based
479 nanocom- posite coatings: I. Dispersion of organophilic montmorillonite in organic
480 solvents. J. Colloid Interface Sci. 278, 26–39.

481 Chtourou, M., Frikha, M.H., Trabelsi, M., 2006. Modified smectitic Tunisian clays used in the
482 formulation of high performance lubricating greases. Appl. Clay Sci. 32, 210–216.

483 Dekany, I., Szanto, F., Weiss, A., Lagaly, G., 1986b. Interactions of hydrophobic
484 layer silicates with alcohol– benzene mixtures: I. Adsorption isotherms. Ber.
485 Bunsenges. Phys. Chem. 90, 422–427.

486 Dolz, M., Hernández, M. J., Delegido, J., 2008. Creep and recovery experimental
487 investigation of low oil content food emulsions. Food Hydrocoll. 22, 421–427.

488 Ebagninin, K. W., Benchabane, A., Bekkour, K., 2009. Rheological
489 characterization of poly(ethylene oxide) solutions of different molecular weights. J.
490 Colloid Interface Sci. 336, 360–367.

491 Gai, K., Avellan, A., Hoelen, T. P., Lopez-Linares, F., Hatakeyama, E. S., Lowry, G.
492 V., 2019. Impact of mercury speciation on its removal from water by activated carbon
493 and organoclay. Water Res.157, 600–609.

494 Geng, T., Qiu, Z., Zhao, C., Zhang, L., and Zhao, X., 2019. Rheological study on the
495 invert emulsion fluids with organoclay at high aged temperatures. Colloids and
496 Surfaces A: Physicochem. Eng. Asp. 573, 211–221.

497 Gherardi, B., Tahani, A., Levitz, P., Bergaya, F., 1996. Sol/gel phase diagrams of
498 industrial organo-bentones in organic media. Appl. Clay Sci. 11, 163–170.

499 Hato, M. J., Zhang, K., Ray, S. S., Choi, H. J., 2011. Rheology of organoclay
500 suspension. Colloid Polym. Sci. 289, 1119–1125.

501 Herzhaft, B., Rousseau, L., Neau, L., Moan, M., Bossard, F., 2003. Influence of
502 Temperature and Clays / Emulsion Microstructure on Oil-Based Mud Low Shear Rate
503 Rheology. Soc. Pet. Eng. 8, 3–10.

504 Jaber, M., Miehé-Brendlé, J., 2009. Organoclays. Preparation, Properties and
505 Applications. Ordered Porous Solids. 31–49.

506 Jayaraj, S., Egodage, S. M., Walpalage, S., 2018. New approach for preparation of dry
507 natural rubber nanocomposites through acid-free co-coagulation: Effect of organoclay
508 content. J. Appl. Polym. Sci. 135, 28, 46502.

509 Jia, Y., Peng, K., Gong, X., Zhang, Z., 2011. Creep and recovery of
510 polypropylene/carbon nanotube composites. Int. J. Plast. 27, 1239–1251.

511 Jordan, J.W., 1949. Organophilic bentonites I. Swelling in organic liquids. J. Phys. Colloid
512 Chem. 53, 294–306.

513 Kelessidis, V. C., Maglione, R., Tsamantaki, C., and Aspirtakis, Y., 2006. Optimal
514 determination of rheological parameters for Herschel–Bulkley drilling fluids and impact
515 on pressure drop, velocity profiles and penetration rates during drilling. J. Pet. Sci. Eng.
516 53, 203–224.

517 Cavalcanti, J.V.F.L., Abreu, C.A.M., Carvalho, M.N., Sobrinho, M.A.M., Benachour,
518 M., Baraúna, O.S., 2012. Removal of effluent from petrochemical wastewater by
519 adsorption using organoclay. Petrochemicals, Intech. 277-294.

520 Lagaly, G., 1981. Characterization of clays by organic compounds. Clay Miner. 16, 1–21.

521 Lagaly, G., Malberg, R., 1990. Disaggregation of alkylammonium montmorillonites in
522 organic solvents. Colloids Surf. 49, 11–27.

523 Luckham, P. F., Rossi, S., 1999. The colloidal and rheological properties of bentonite
524 suspensions. Adv. Colloid Interface Sci. 82, 43–92.

525 Jhon, M. S., Kwon, T. M., Choi, H. J., Karis, T. E., 1996. Microrheological Study of
526 Magnetic Particle Suspensions. Ind. Eng. Chem. Res. 35, 3027–3031.

527 Merinska, D., Malac, Z., Pospisil, M., Weiss, Z., Chmielova, M., Capkova, P.,
528 Simonik, J., 2002. Polymer/clay nanocomposites on MMT/ODTA intercalates.
529 Comp. Interf. 9, 529–540.

530 Moraru, V.N., 2001. Structure formation of alkylammonium montmorillonites in organic
531 media. Appl. Clay Sci. 19, 11–26.

532 Ben Moshe, S. and Rytwo, G., 2018. Thiamine-based organoclay for phenol removal
533 from water. Appl. Clay Sci. 155, 50–56.

534 Mourchid, A. and Levitz, P., 1998. Long-term gelation of laponite aqueous dispersions. Phys.
535 Rev. E. 57, 4887.

536 Murray, H.H., 2000. Traditional and new applications for kaolin, smectite, and palygorskite: a
537 general overview. Appl. Clay Sci. 17, 207–221

538 Murray, H.H., 2007. Applied clay mineralogy: occurrences, processing, and application of
539 kaolins, bentonites, palygorskite-sepiolite, and common clays. Developments in clay science,
540 vol. 2, Elsevier.

541 Paiva, L.B.D., Morales, A.R., Díaz, F.R.V., 2008. Organoclays: properties,
542 preparation and ap- plications. Appl. Clay Sci. 42, 8–24.

543 Ragouilliaux, A., 2007. Etude rhéophysique de systèmes émulsions inverses / argile
544 organophile . Applications au boues de forage pétrolier. Docteur de l'université Pièrre et
545 Marie Curie, France.

546 Ramos-Tejada, M. M., Arroyo F. J., Perea, R., and Durán, J. D. G., 2001. Scaling
547 Behavior of the Rheological Properties of Montmorillonite Suspensions: Correlation
548 between Interparticle Interaction and Degree of Flocculation. J. Colloid Interface
549 Sci. 235, 251–259.

550 Ramsay, J. D., 1986. Colloidal properties of synthetic hectorite clay dispersions: I.
551 Rheology. J. Colloid Interface Sci. 109, 441–447.

552 Ray, S.S., 2010. A new possibility for microstructural investigation of clay-based
553 polymer nanocomposite by focused ion beam tomography. Polymer. 51,17, 3966-
554 3970.

555 Rooki, R., Doulati, Ardejani, F., Moradzadeh, A., Mirzaei, H., Kelessidis, V.C.,
556 Maglione R., Norouzi M., 2012. Optimal determination of rheological parameters for
557 herschel-bulkley drilling fluids using genetic algorithms (GAs). Korea-Australia Rheol. J.
558 24, 163–170.

559 Shakeri, F., Nodehi, A., Atai, M., 2019. PMMA/double-modified organoclay
560 nanocomposites as fillers for denture base materials with improved mechanical
561 properties. J. Mech. Behav. Biomed. Mater. 90, 11–19.

562 Slabaugh, W.H., Hiltner, P.A., 1968. Swelling ofalkylammoniummontmorillonites. J. Phys.
563 Chem. 12, 4295–4298.

564 Vaia, R.A., Teukolsky, R.K., Giannelis, E.P., 1994. Interlayer structure and
565 molecular environment of alkylammonium layered silicates. Chem. Mater. 6,
566 1017–1022.

567 Zhang, L.-M., Jahns, C., Hsiao, B. S., and Chu, B., 2003. Synchrotron SAXS/WAXD and
568 rheological studies of clay suspensions in silicone fluid. J. Colloid Interface Sci., 266,
569 339–345.

570 Zhong, Y.,Wang, S.Q., 2003. Exfoliation and yield behavior in nanodispersions
571 of organically modified montmorillonite clay. J. Rheol. 47, 483–495.

572 Zhuang, G., Zhang, Z., Sun, J., Liao, L., 2016. The structure and rheology of organo-
573 montmorillonite in oil-based system aged under different temperatures. Appl. Clay Sci.
574 124, 21–30.

575 Zhuang, G., Zhang, H., Wu, H., Zhang, Z., Liao, L., 2017. Influence of the surfactants'
576 nature on the structure and rheology of organo-montmorillonite in oil-based drilling
577 fluids. Appl. Clay Sci. 135, 244–252.

578 Zhuang, G., Zhang, Z., Yang, H., Tan, J., 2018. Structures and rheological properties of
579 organo-sepiolite in oil-based drilling fluids. Appl. Clay Sci. 154, 43–51.

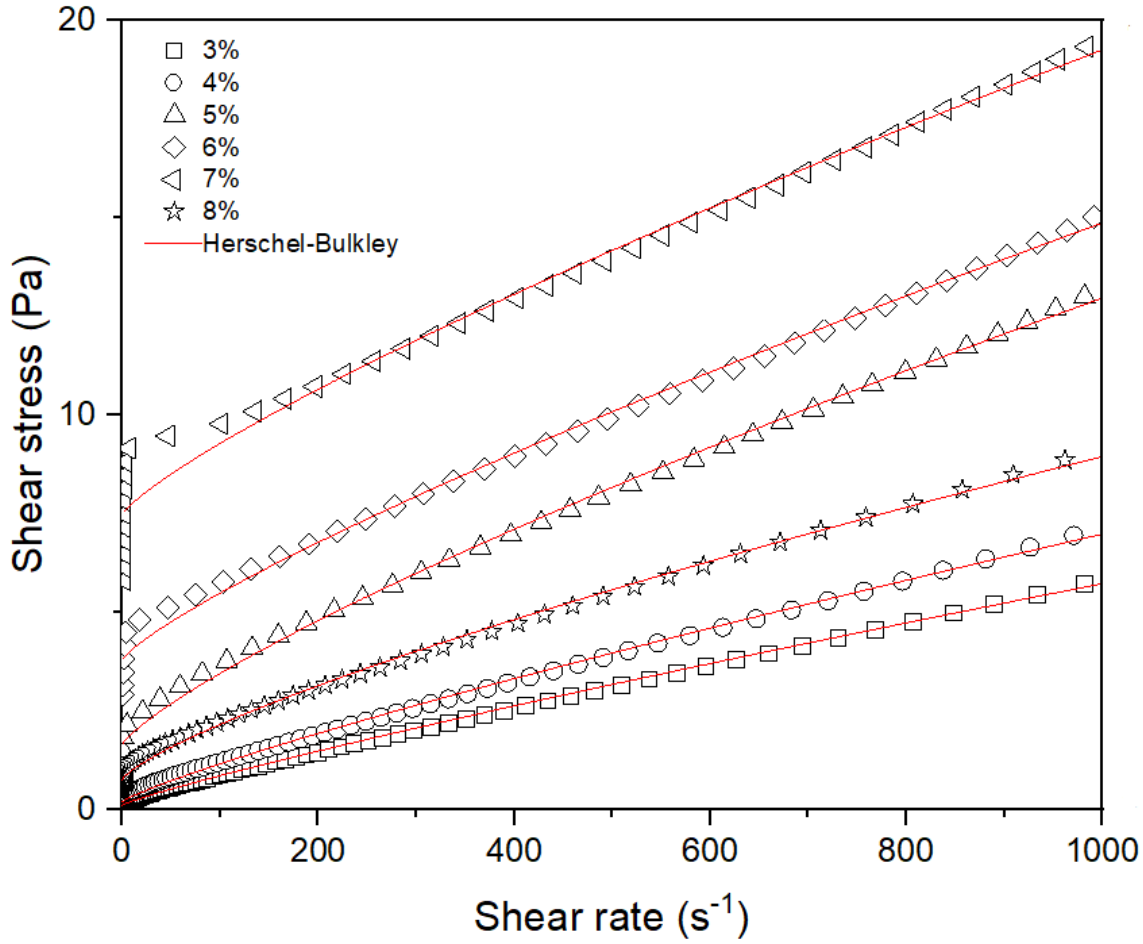

Fig. 1. Flow curves of modified hectorite dispersion correlated using the Herschel-Bulkley Model.

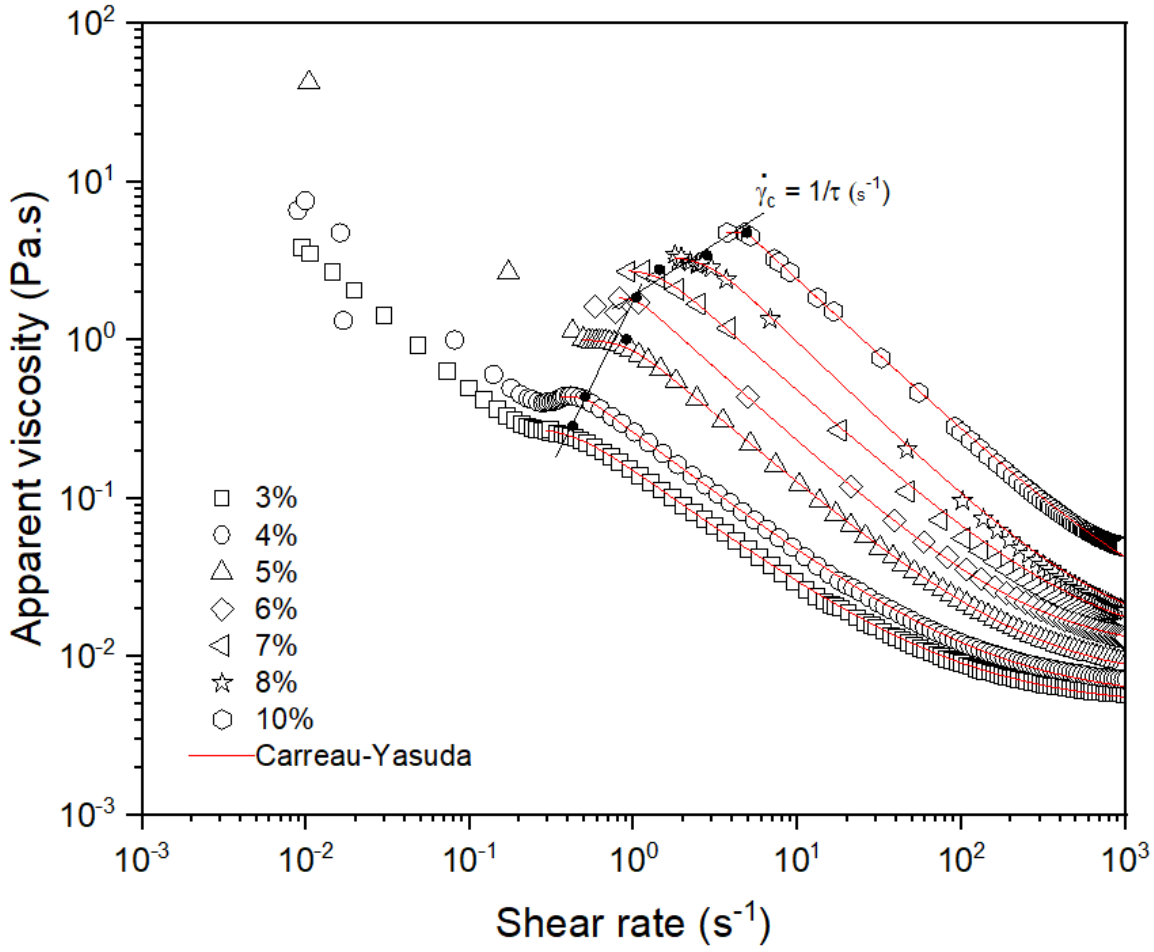

Fig. 2. Flow curves of modified hectorite dispersion correlated using the Carreau-Yasuda Model.

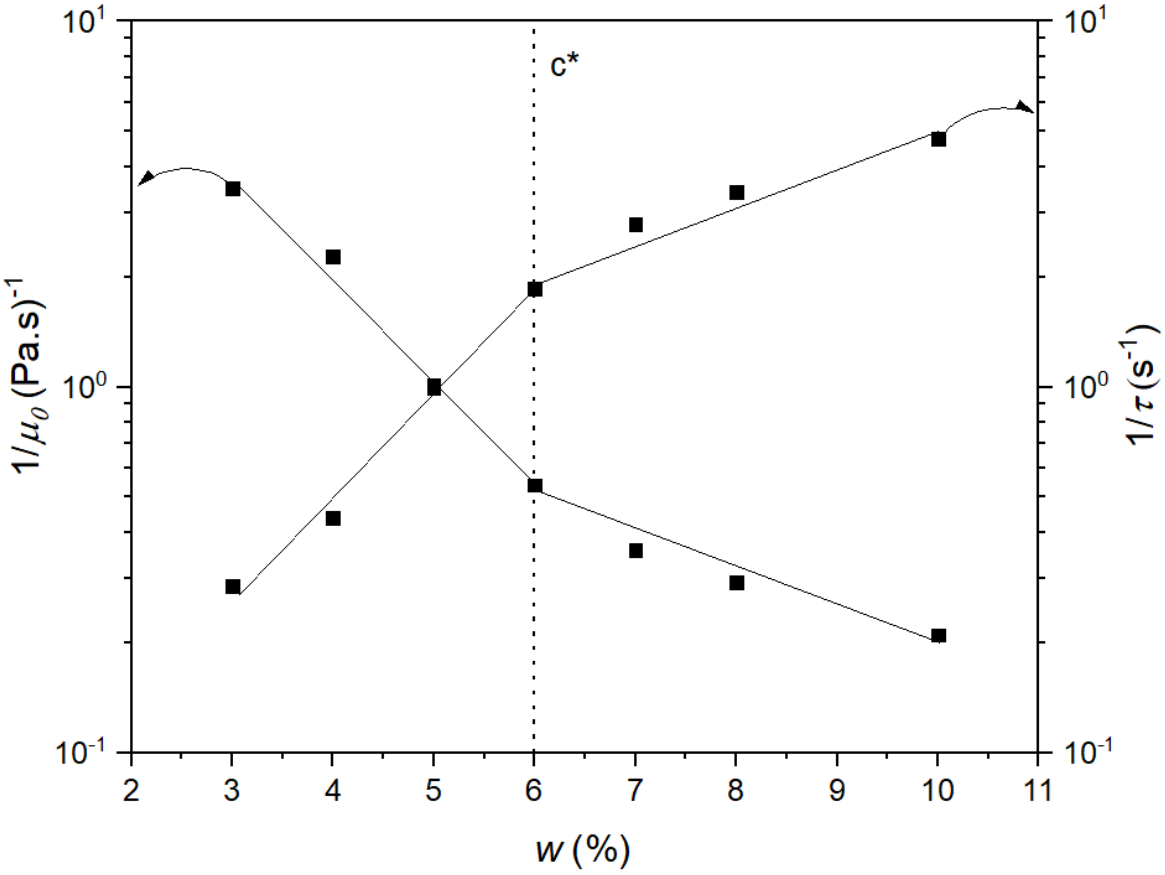

Fig. 3. Critical shear rate and the reciprocal of the zero-shear-rate viscosity as a function of organoclay loading.

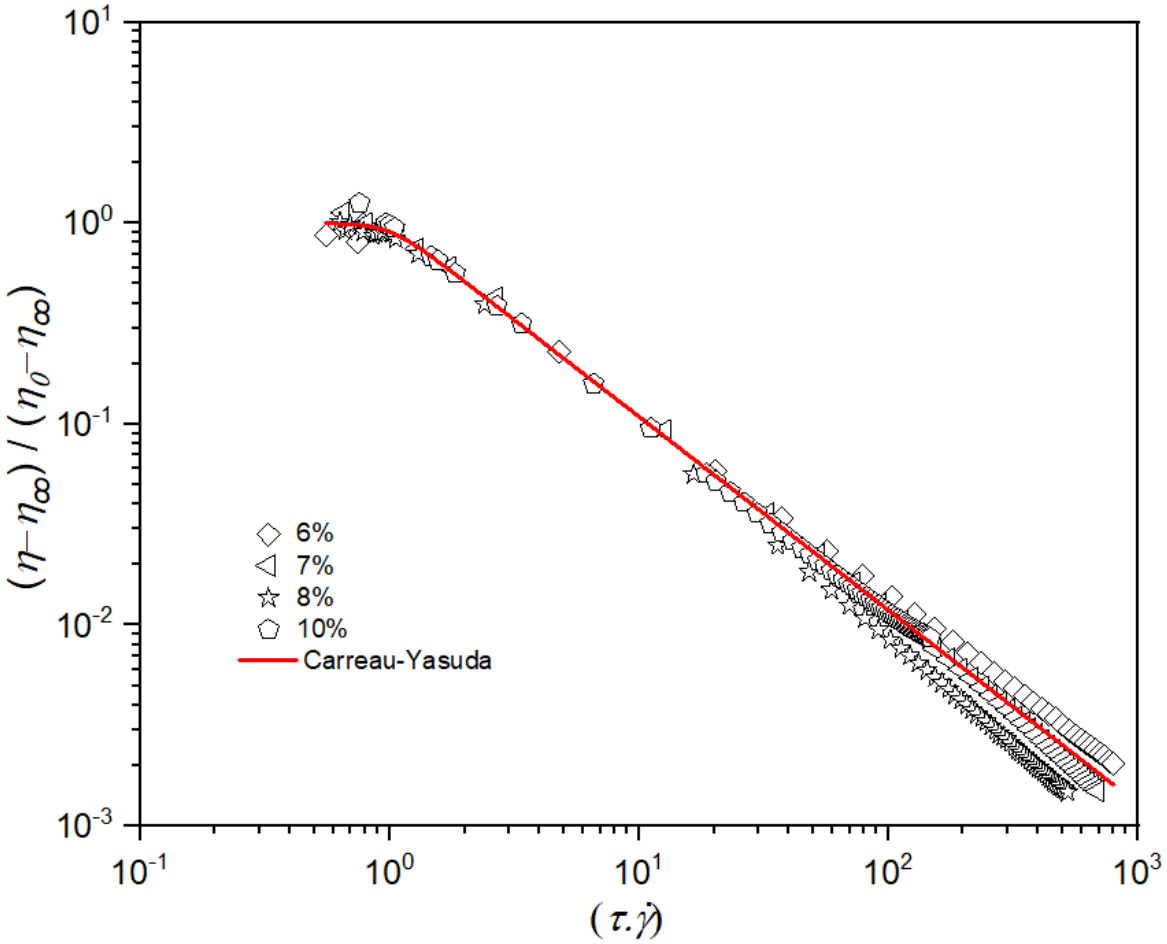

Fig. 4. Dimensionless viscosity as a function of dimensionless shear rate, using the Carreau-Yasuda model parameters.

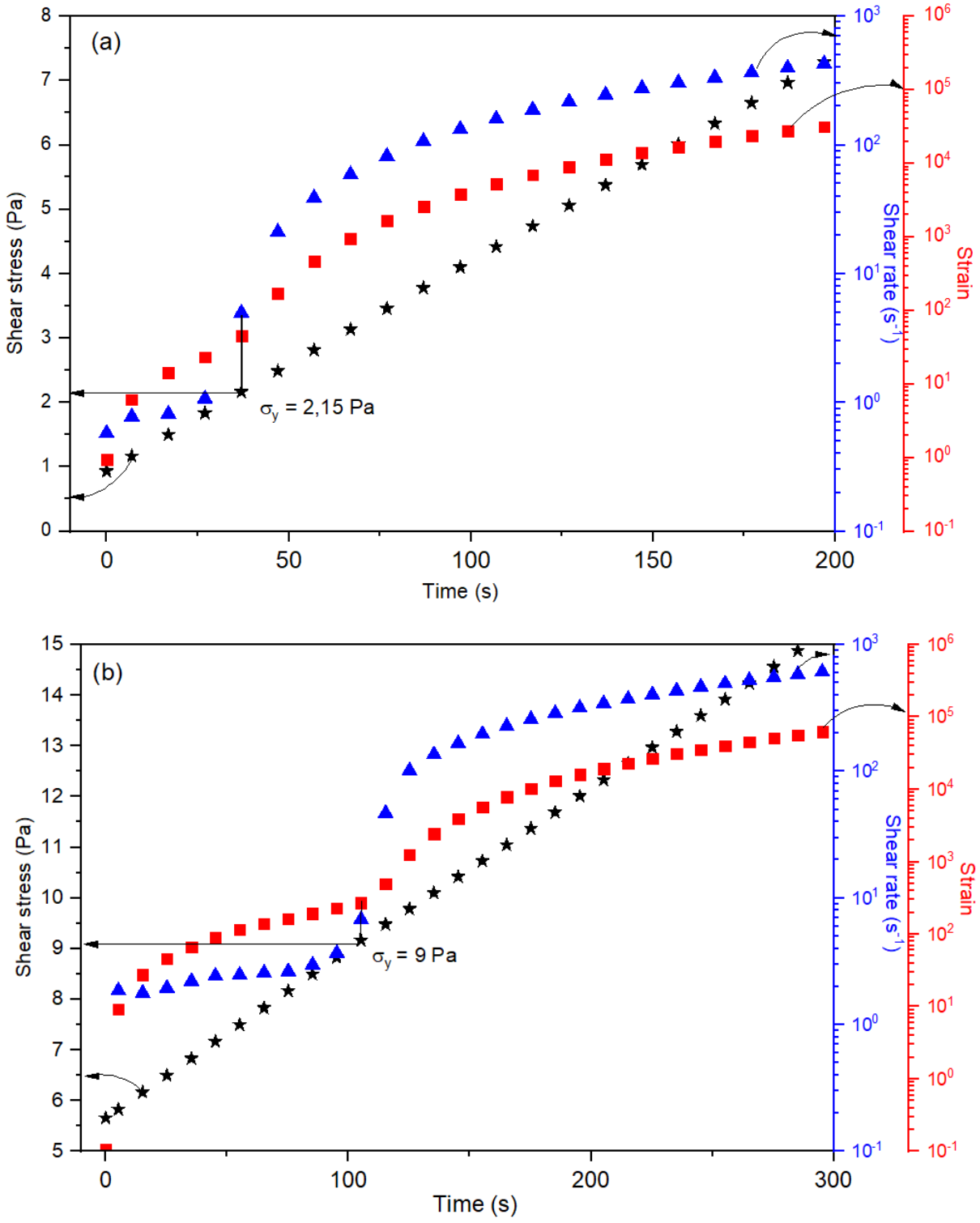

Fig. 5. Determination of yield stress by plotting shear stress, shear rate and strain as a function of time for organoclay loadings of 6 wt% (a) and 8 wt% (b).

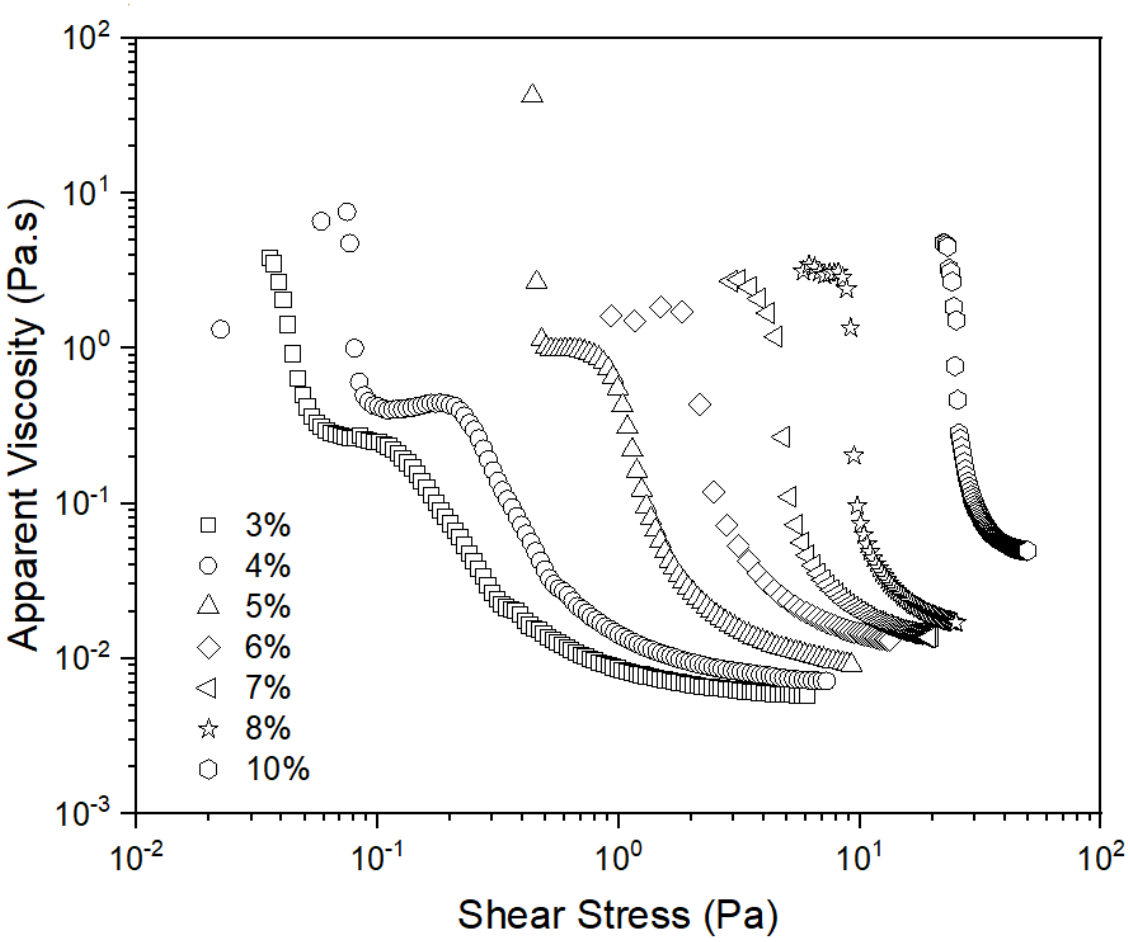

Fig. 6. Apparent viscosity as a function of Shear stress.

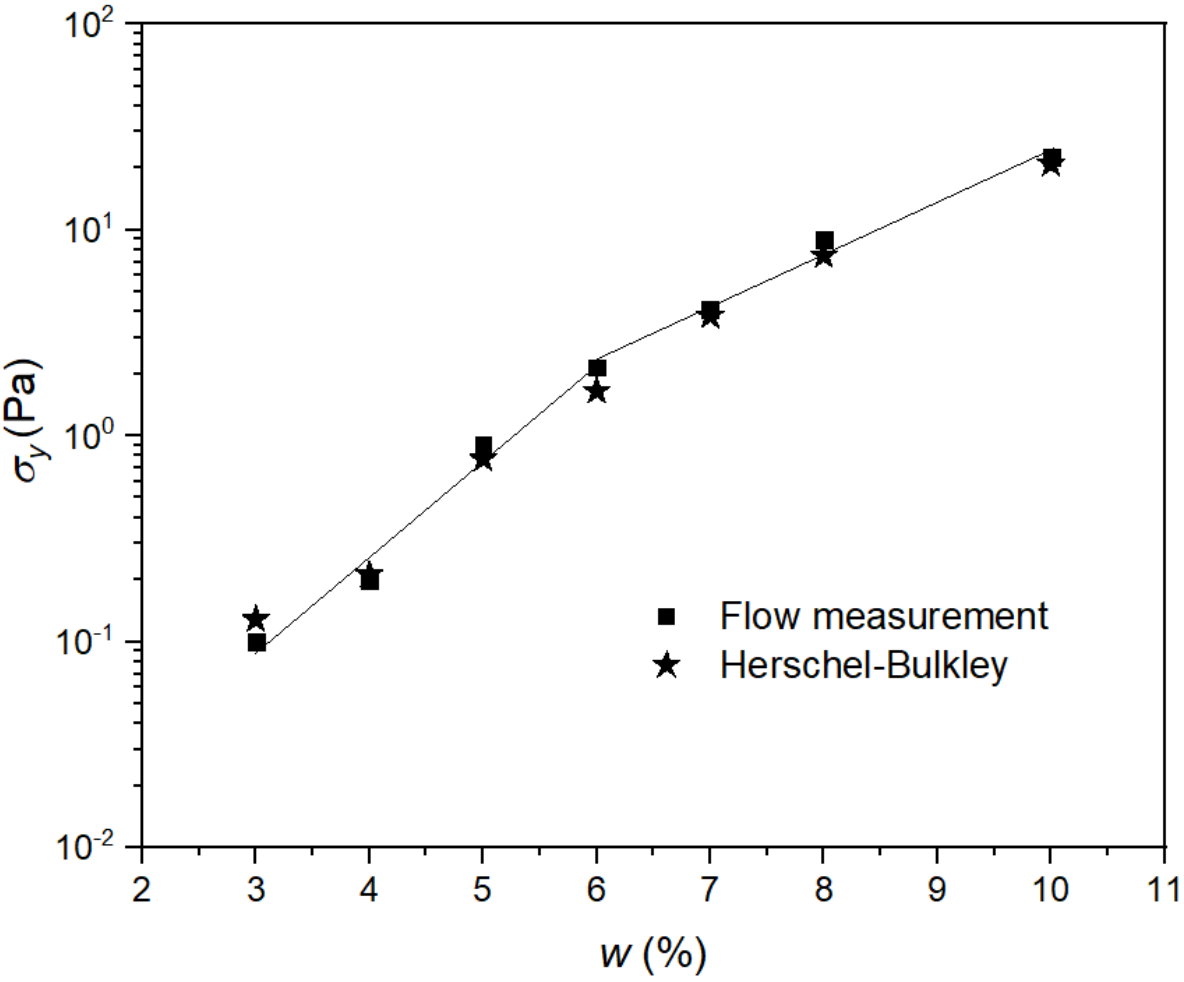

Fig. 7. Yield stress obtained from the flow measurements and the Herschel-Bulkley model as a function of clay loading fitted using Eq (2).

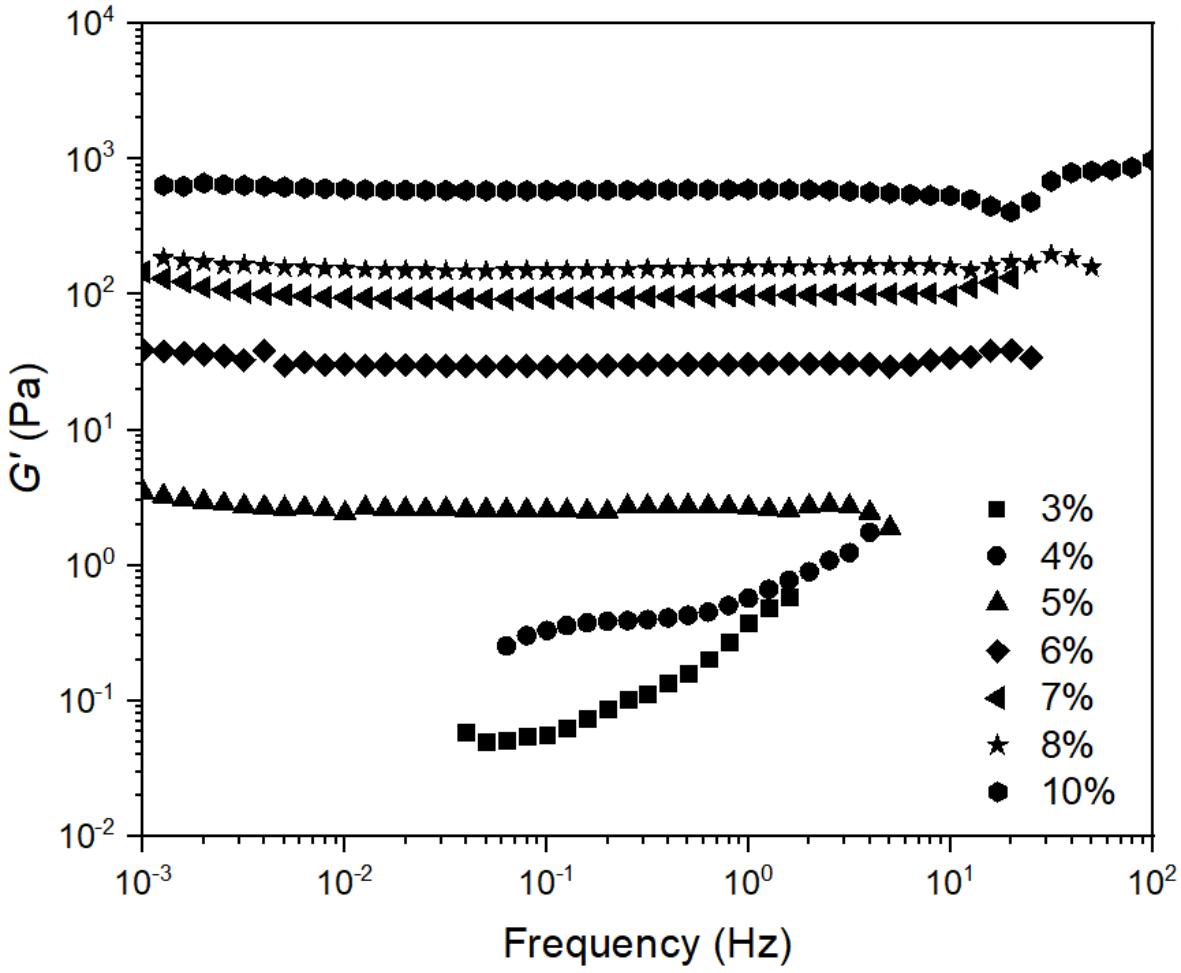

Fig. 8. Storage modulus as a function of organoclay loading at 0,1 Hz.

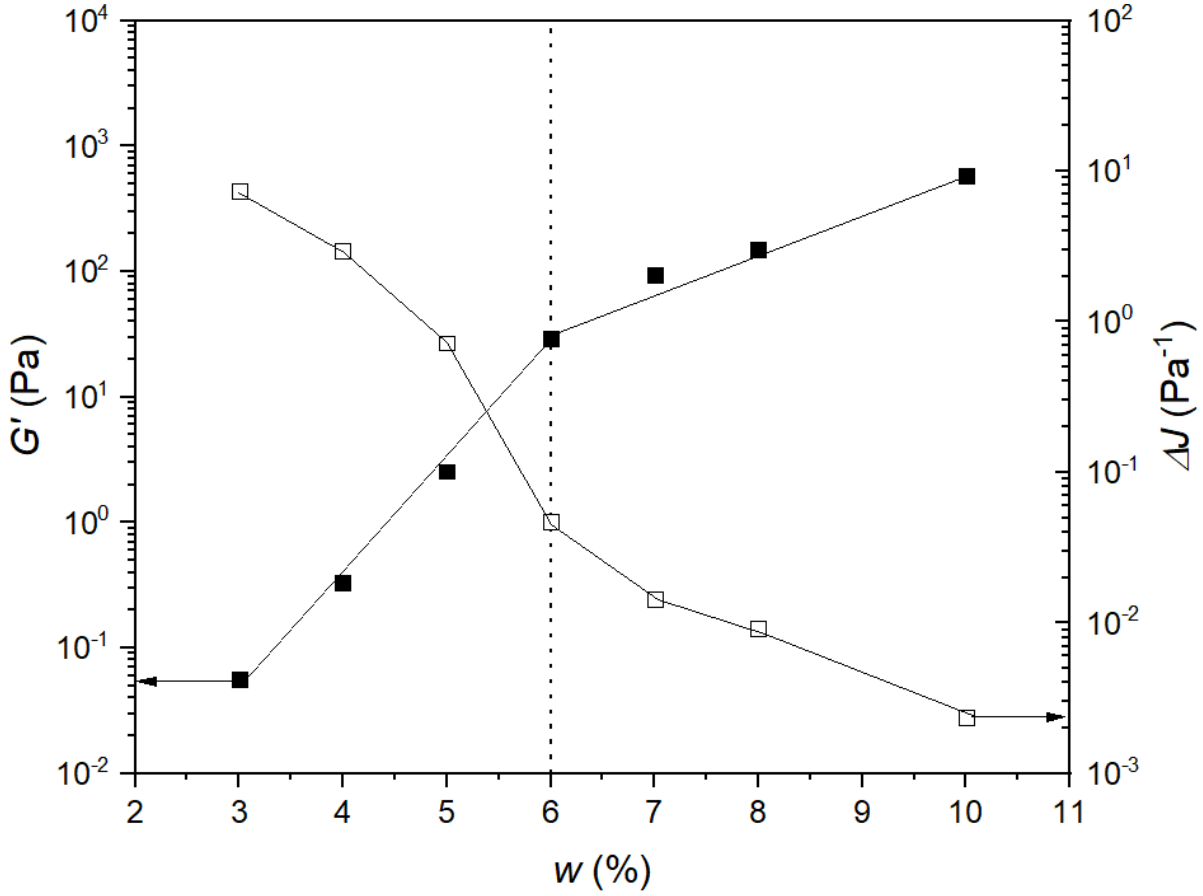

Fig. 9. Storage modulus and recovery elastic index as a function of organoclay loading.

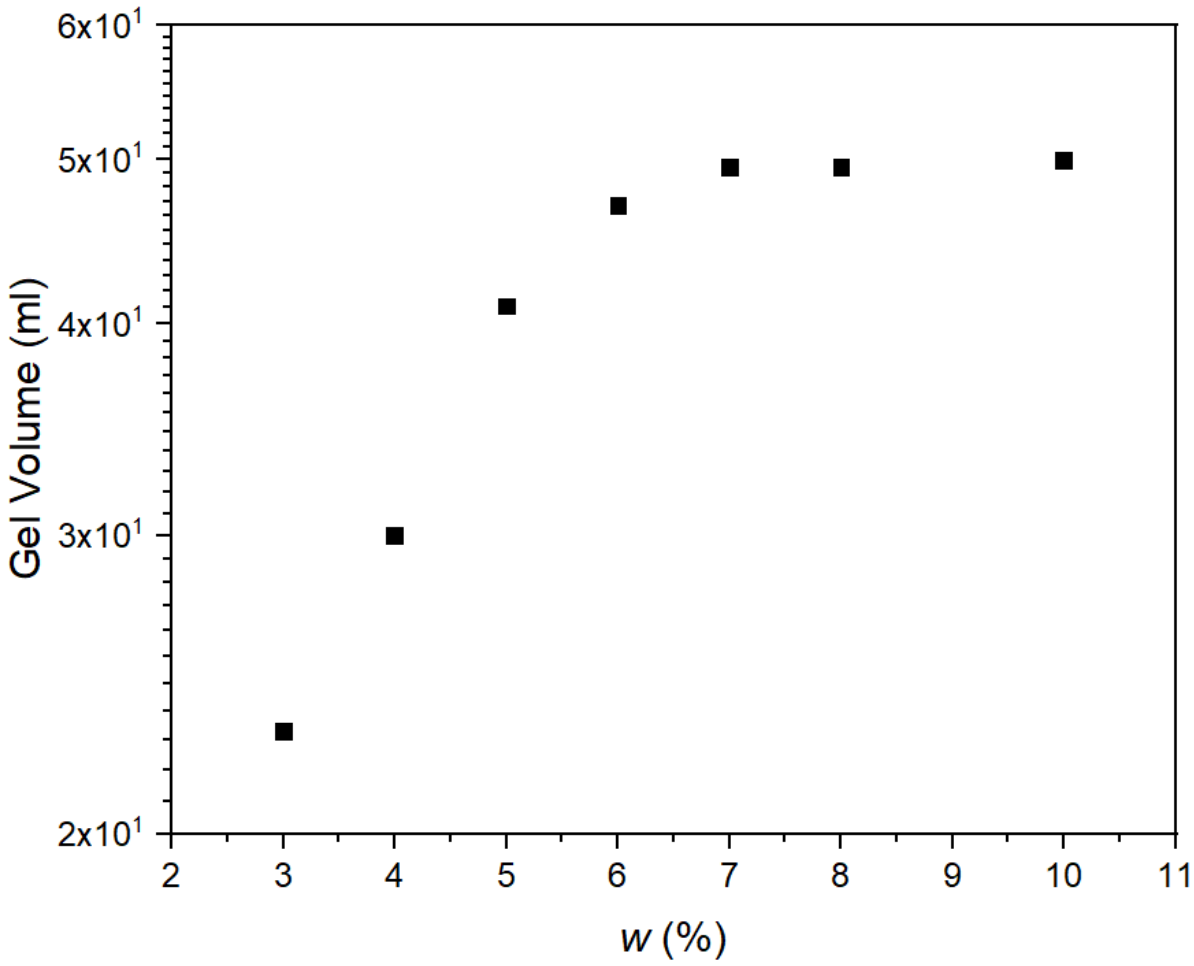

Fig. 10. Gel volume as a function of organoclay loading.

Concentration	α [-]	K [Pa s^{-1}]	σ_c [Pa]	R^2
3%	0.877 ± 0.006	0.013 ± 0.001	0.128 ± 0.007	0.999
4%	0.847 ± 0.008	0.020± 0.001	0.21 ± 0.01	0.998
5%	0.77 ± 0.01	0.040 ± 0.004	0.77 ± 0.03	0.996
6%	0.80 ± 0.02	0.047 ± 0.006	1.65 ± 0.09	0.996
7%	0.82 ± 0.03	0.039 ± 0.007	3.8 ± 0.1	0.995
8%	0.82 ± 0.05	0.04 ± 0.01	7.5 ± 0.2	0.990
10%	0.91 ± 0.05	0.04 ± 0.01	20.9 ± 0.4	0.995

Table 1. Rheological parameters of the Herschel-Bulkley model.

Concentration	τ [s]	n [-]	a [-]	η_0 [Pa.s]	η □ [Pa.s]	R^2
3%	2.35 ± 0.02	0.235 ± 0.007	3.3 ± 0.2	0.286 ± 0.002	0.004 ± 0.001	0.99
4%	1.99 ± 0.01	0.219 ± 0.006	12.6 ± 1.5	0.439 ± 0.001	0.005 ± 0.001	0.99
5%	1.11 ± 0.01	0.12 ± 0.01	4.9 ± 0.2	1.010 ± 0.003	0.007 ± 0.001	0.99
6%	0.964 ± 0.004	0.063 ± 0.003	10.3 ± 0.5	1.854 ± 0.001	0.010 ± 0.001	0.99
7%	0.70 ± 0.01	0.083 ± 0.002	5.3 ± 0.7	2.79 ± 0.03	0.011 ± 0.002	0.99
8%	0.36 ± 0.03	0.070 ± 0.005	4.3 ± 1.2	3.42 ± 0.09	0.01 ± 0.01	0.99
10%	0.204 ± 0.001	0.039 ± 0.004	34.5 ± 4.3	4.76 ± 0.01	0.014 ± 0.001	0.99

Table 2. Rheological parameters of the Carreau-Yasuda model.

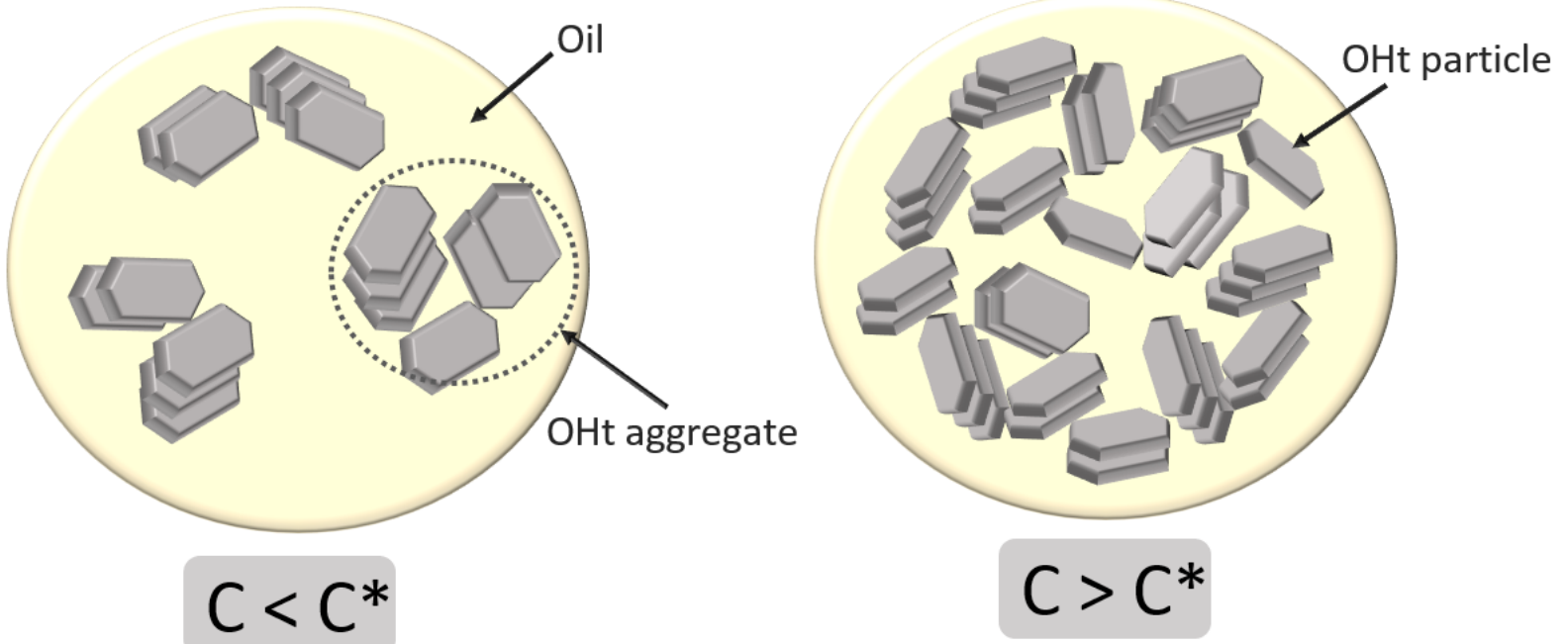
Oil
OHt aggregate
OHt particle
C < C*
C > C*